

Baryonic decays of the $\psi(3095)$

I. Peruzzi,* M. Piccolo,* M. S. Alam, A. M. Boyarski, M. Breidenbach, G. J. Feldman, G. Hanson, J. A. Jaros, D. Lüke, V. Lüth, H. L. Lynch,† J. M. Paterson, T. P. Pun, P. A. Rapidis, B. Richter, R. H. Schindler, R. F. Schwitters, J. Siegrist, and W. Tanenbaum‡

Stanford Linear Accelerator Center, Stanford University, Stanford, California 94305

G. Goldhaber, A. D. Johnson, G. S. Abrams, W. Chinowsky, J. A. Kadyk,§ R. J. Madaras, H. K. Nguyen,¶ G. H. Trilling, and J. E. Wiss¶

Lawrence Berkeley Laboratory and Department of Physics, University of California, Berkeley, California 94720

(Received 3 January 1978)

We have measured the branching ratios for a number of $\psi(3095)$ decay modes involving protons or Λ 's. We present an analysis of the properties of these final states, which provides information on $\psi(3095)$ quantum numbers and the presence of resonances in the final states.

I. INTRODUCTION

The $\psi(3095)$, hereafter denoted by the symbol ψ , is now usually interpreted as a bound state of a charmed quark and a charmed antiquark ($c\bar{c}$). The discovery of the charmed mesons D and D^* gives considerable support to this interpretation.^{1,2} The study of the exclusive states from ψ decay is therefore of great interest: The relative branching ratios and other properties can in fact be compared with those expected from a $c\bar{c}$ bound state. Since its discovery several decay modes of the ψ have been measured. We have already reported³ studies of the multipion decays of the ψ which established that (a) isospin is conserved in ψ hadronic decays and (b) the ψ has isospin zero as expected from the $c\bar{c}$ model. We have also reported⁴ measurements of the branching ratios for a number of mesonic decays of the ψ containing kaons, ω , ϕ , etc. This study showed that the ψ follows the general pattern of behavior expected for the decay of an SU(3) singlet via an SU(3)-symmetric interaction.

In this paper we present the branching ratios for a number of baryonic decay channels of the ψ . The sum of these decays accounts for a few percent of all ψ decays. Their study presents several interesting features. The angular distribution of the $p\bar{p}$ and $\Lambda\bar{\Lambda}$ collinear pairs gives information about the form of the baryon coupling to the ψ . The comparison of the $\Lambda\bar{\Lambda}$ and $\Sigma\bar{\Lambda}$ decay rates is an independent measure of the ψ isospin, and the comparison of $p\bar{p}$ and $\Lambda\bar{\Lambda}$ decay rates provides additional information on the SU(3) character of ψ decays. The relative amount of $p\bar{p}\eta$ and $p\bar{p}\eta'$ compared with $p\bar{p}\pi^0$ and $p\bar{p}\omega$ is a possible test of the hypothesis that the η and η' mesons have a non-zero $c\bar{c}$ quark content.⁵

II. THE APPARATUS

The data presented here are based on the analysis of approximately 150 000 hadronic decays of the ψ , recorded by the SLAC-LBL magnetic detector operating at the SLAC electron-positron colliding-beam facility SPEAR. This sample corresponds to an integrated luminosity of 150 nb^{-1} .

The general properties of the detector have already been published.^{4,6} We will summarize here the relevant elements, with emphasis on the parts which are essential for proton and Λ detection.

Figure 1 shows a cross-sectional view of the detector. The magnet is a solenoid, with a 1-radiation-length-thick coil, coaxial with the beam, 3 m long, 1.7 m in radius, and provides a field of about 4 kG, which is uniform to a few percent.

The momentum and direction of the charged particles produced in the collision region are measured in two cylindrical proportional chambers and four sets of cylindrical wire magnetostrictive spark chambers. Each set of wires has two gaps (4 wire planes), one with a 2° stereo angle and one with a 4° stereo angle.

Just inside the coil are a set of 48 scintillation counters (2.6 m long, 0.23 m wide, at a distance of 1.5 m from the beam), which provide the trigger signals and time-of-flight (TOF) information for particle identification.

Outside the coil there is a hodoscope of 24 lead-scintillator shower counters, each consisting of a sandwich of five 0.64-cm-thick (about 1-radiation-length) lead sheets and five 0.64-cm-thick plastic scintillator sheets. These counters are 0.48 m wide and have an active length of 3.10 m. Their signals are sent to the trigger circuitry and are also used to identify electrons and photons. Outside the shower counters there is the iron flux return and the muon-identification system. The trigger normally requires signals in the pipe

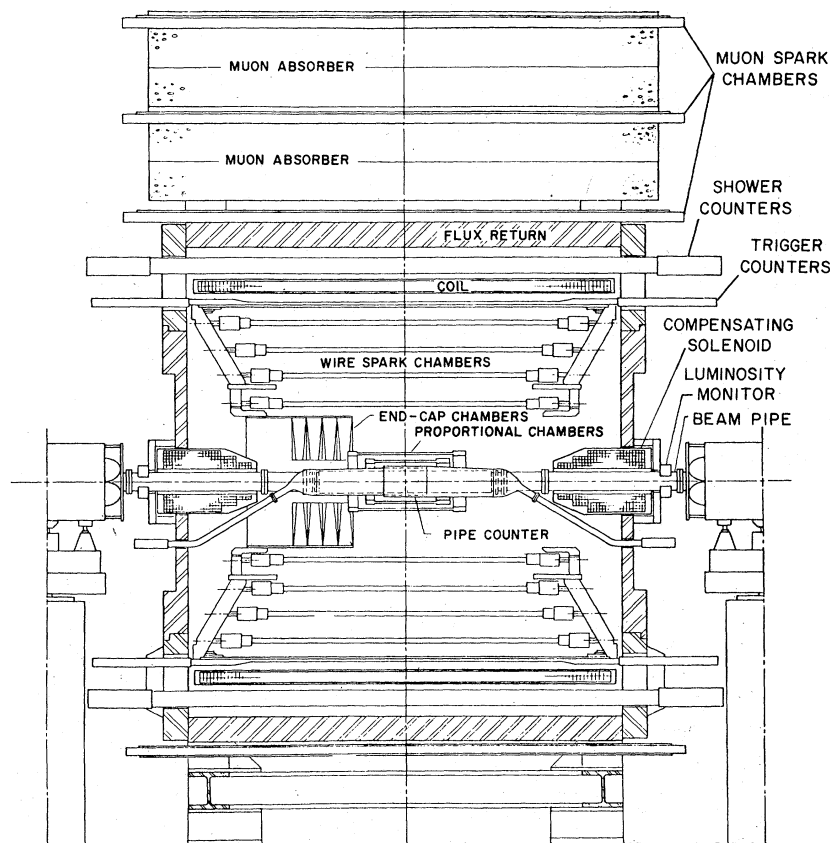


FIG. 1. A cross-sectional view of the SLAC-LBL magnetic detector.

counters (which surround the vacuum chamber) in time with the beam crossing and two or more coincidences of trigger counters with a backing shower counter. To satisfy this trigger condition, an event must have two or more charged particles with momenta ≥ 200 MeV/c (if pions). In the case of protons this momentum threshold is higher because to reach the trigger counters a proton must have at least ~ 350 MeV/c (the beam pipe, the pipe counters, and the proportional chambers have a combined thickness of 1.9 g/cm²). In order to give a pulse in both the trigger counter and the associated shower counter a proton must have at least ~ 680 MeV/c. On the other hand, an antiproton which reaches the trigger counter has close to unit probability to give a signal in the associated shower counters because of the high likelihood of interaction. In order to symmetrize the trigger for the $p\bar{p}$ inelastic pairs, the more recent sample of data (about $\frac{2}{3}$ of the total) has been taken with a looser trigger requirement, i.e., two signals in the trigger counters, but only one trigger-shower coincidence.

The momentum resolution for tracks which originate in the beam interaction region is $\sigma(p)/p = 0.013 \times p$ (in GeV/c). It is poorer by about a fac-

tor 2 for the decay products of long-lived particles such as Λ 's, since in this case the beam-beam interaction point cannot be used as a constraint in the fit to the track. Below 110 MeV/c the resolution without the beam position deteriorates rapidly, being $\sim 12\%$ at 75 MeV/c and $\sim 20\%$ at 55 MeV/c, since the track no longer traverses all the chambers.

III. PARTICLE IDENTIFICATION

A. Protons

The protons and antiprotons are identified on the basis of the joint measurement of time of flight (TOF), momentum, and path length of the tracks.

The TOF is calibrated using e^+e^- collinear events from Bhabha scattering. A number of software corrections are applied to the measured TOF in order to optimize the resolution of the system. The time measured from each photomultiplier is corrected using the pulse-height information. The values obtained from the two photomultipliers of the same counter are then averaged. This average is performed taking into account the point of impact on the counter. Calibration constants for each counter are monitored on a run-by-run basis to

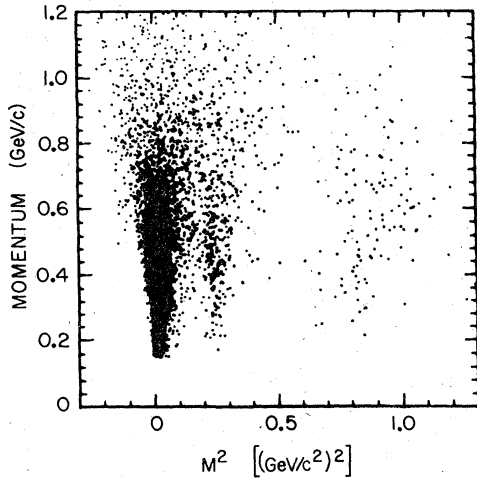


FIG. 2. Mass squared for each track, reconstructed from TOF and momentum measurements versus momentum.

maintain the resolution at its optimal value over long periods of time. Figure 2 shows a typical plot of the mass squared obtained from the measurement of TOF and path length as a function of the track momentum. The three bands correspond to pions, kaons, and protons. At a momentum of 1.23 GeV/c, corresponding to $p\bar{p}$ pair production from the ψ and hence to the maximum possible proton momentum, the difference in time between a kaon and a proton is about 2.5 standard deviations (s.d.) (the resolution of the TOF is typically 0.35 nsec).

To select the sample of events to which this analysis refers, we have used the following criteria: We have selected all ψ events which contain at least one track with momentum less than 1.35 GeV/c whose time of flight corresponds to a proton within 4 s.d. This selection leaves a small kaon contamination, which is, however, negligible for events which have both a proton and antiproton candidate. In some cases, as for the decay $\psi \rightarrow p\bar{n}\pi^-$, only one proton is produced; the background from misidentified kaons is then eliminated by a one-constraint (1C) fit. In the case of $p\bar{p}$ pair production or the decay into $p\bar{p}\pi^+\pi^-$, a 4C fit can be performed and there is no need of TOF identification.

B. Λ 's

In our detector we can identify the Λ ($\bar{\Lambda}$) as a peak in the $p\pi^-$ ($\bar{p}\pi^+$) invariant-mass distribution. Figure 3(a) shows the $p\pi^-$, $\bar{p}\pi^+$ mass distribution where the proton is identified by a loose mass cut [$m^2 > 0.4 \text{ GeV}/c^2$]. The $\Lambda + \bar{\Lambda}$ signal contains 1559 ± 62 events with an rms mass resolution of 5 MeV. We

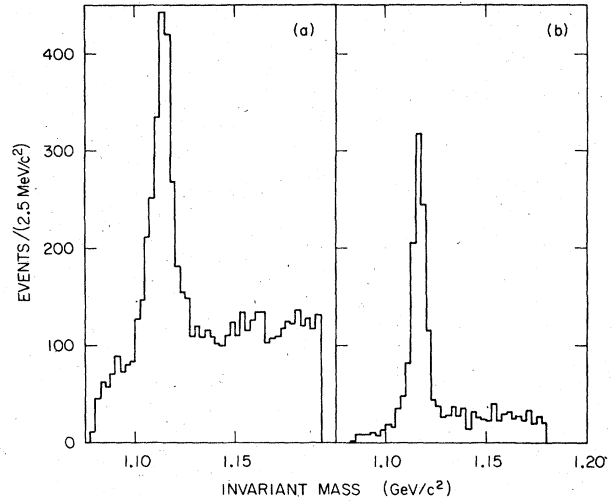


FIG. 3. Invariant-mass spectra for $p\pi^-$ and $\bar{p}\pi^+$ combinations with (a) no cuts applied and (b) cuts on the reconstructed vertex, as explained in the text.

define a Λ as a $(p\pi)^0$ pair with invariant mass between 1.105 and 1.125 GeV/c²; the signal fraction in this region is 60%.

When the statistics are sufficient, a better signal-to-background ratio can be achieved with the following procedure: For each $p\pi^-$ or $\bar{p}\pi^+$ pair of tracks we determine the projection of the intersection point in the x - y plane (the one perpendicular to the beams). In order to ensure a good resolution in the vertex position, pairs which have a projected opening angle of less than 10° or more than a 170° are rejected. Usually for each pair of tracks there are two intersections, one of which, the unphysical one, lies far away from the interaction region and can be easily eliminated. In case of ambiguity, the third coordinate is used and the solution for which the intersection of the tracks is closer in the z direction (along the beam line) is chosen. A cut of 16 cm on the distance of the vertex from the interaction point is applied, which corresponds to the radius of the inner proportional chamber. The intersection is then checked using the third coordinate: Tracks which are separated by more than 16 cm are rejected. The momentum of each track is then calculated at the intersection point, and the angle between the total momentum and the vector pointing to the vertex is checked. If the distance of the vertex is less than 6 mm this angle is subject to substantial measurement error, so all the pairs of tracks in this category are accepted. Otherwise a cut of 20° is applied. The $(p\pi)^0$ invariant mass distribution obtained with these criteria is shown in Fig. 3(b), where the $\Lambda + \bar{\Lambda}$ peak contains 907 ± 37 events. The rms resolu-

tion is 3 MeV and the signal fraction in the mass interval 1.105 to 1.125 GeV/c² is 82%. These cuts thus reduce the background from 40% to 18%.

IV. EFFICIENCY CALCULATION

In order to translate the number of events for a given process into branching ratios, the overall efficiency has been calculated using a Monte Carlo technique. The geometry of the detector, the measurement resolution, the trigger requirements, the counter inefficiencies, and all the other known experimental effects are simulated in the Monte Carlo program. The simulated events are then analyzed with the same technique used for the real events in order to take into account all of the selection criteria. The fact that in each case we consider a specific channel removes much of the model dependence of such efficiency calculations. We have, however, included in the quoted errors on the branching ratios a 10% systematic uncertainty in the value of the efficiency. In addition, there is a 15% uncertainty in the overall efficiency for ψ -hadrons which is not explicitly included in the quoted errors.

V. DECAYS INVOLVING NONSTRANGE BARYONS

The results of the branching ratio determination for the decays of the ψ into nonstrange baryons are

summarized in Table I, along with the number of events found for each final state and the respective detection efficiency.

In the following discussion we describe the criteria by which the samples used in these determinations were selected. Unless otherwise specified, we will always sum each final state with its charge conjugate.

A. $\psi \rightarrow p\bar{p}$

The pair production of protons from the ψ has already been reported.⁷⁻⁹ This process is easily identified within the collinear two-prong events without use of the TOF. Figure 4 shows the mass for these events (after removing the electron pairs), reconstructed from the measurement of the average momentum of the two tracks: $M^2 = E_B^2 - p^2$, where E_B is the energy of incident e^- or e^+ beam. The peak centered near zero corresponds to the muon pairs; the other peak is centered at the proton mass and contains 331 ± 18 events. This translates into a branching fraction for $\psi \rightarrow p\bar{p}$ of $(2.2 \pm 0.2) \times 10^{-3}$ in good agreement with the measurements of Refs. 8 and 9. Figure 5 shows the angular distribution of the proton pairs with respect to the beam axis. The angular distribution of the muon pairs, which has been measured to be proportional to $1 + \cos^2\theta$, is shown in the same plot

TABLE I. Decay modes of the $\psi(3095)$ to states containing baryons.

Decay	Topology	Number of events	Efficiency	Branching ratio
$p\bar{p}$	2 prongs collinear	331 ± 18	0.38	$(2.2 \pm 0.2) \times 10^{-3}$
$p\bar{n}\pi^-$	$p\bar{n}\pi^-$	194 ± 17	0.22	$(2.16 \pm 0.29) \times 10^{-3}$
$\bar{p}n\pi^+$	$\bar{p}\pi^+$	204 ± 18	0.25	$(2.04 \pm 0.27) \times 10^{-3}$
$p\bar{p}\pi^0$	$p\bar{p}$	109 ± 13	0.27	$(1.00 \pm 0.15) \times 10^{-3}$
$p\bar{p}\gamma$	$p\bar{p}^+$ shower	<8	0.18	$<1.1 \times 10^{-4}$
$p\bar{p}\eta$	$p\bar{p}$	142 ± 19	0.15	$(2.3 \pm 0.4) \times 10^{-3}$
	$p\bar{p}\pi^+$	33 ± 10	0.03	
	$p\bar{p}\pi^+\pi^-$	22 ± 6	0.03	
$p\bar{p}\omega$	$p\bar{p}\pi^\pm$	42 ± 14	0.05	$(1.6 \pm 0.3) \times 10^{-3}$
	$p\bar{p}\pi^+\pi^-$	35 ± 8	0.06	
$p\bar{p}\eta'$	$p\bar{p}\pi^\pm$	19 ± 10	0.025	$(1.8 \pm 0.6) \times 10^{-3}$
	$p\bar{p}\pi^+\pi^-$	21 ± 8	0.03	
$p\bar{p}\pi^+\pi^-$	$p\bar{p}\pi^\pm$	178 ± 25	0.07	$(5.5 \pm 0.6) \times 10^{-3}$
	$p\pi^+\pi^-$	135 ± 24	0.06	
	$p\bar{p}\pi^+\pi^-$	220 ± 16	0.11	
$p\bar{p}\pi^+\pi^-\pi^0 +$ $p\bar{p}\pi^+\pi^-\gamma$ (excluding $p\bar{p}\eta$, $p\bar{p}\omega$, and $p\bar{p}\eta'$)	$p\bar{p}\pi^+\pi^-$	39 ± 14	0.06	$(1.6 \pm 0.6) \times 10^{-3}$
$\Lambda\bar{\Lambda}$	$\Lambda + X$	153 ± 24	0.33	$(1.1 \pm 0.2) \times 10^{-3}$
	$\Lambda\bar{\Lambda}$	43 ± 8	0.10	
$\Sigma^0\bar{\Sigma}^0$	$\Lambda\bar{\Lambda}$	52 ± 10	0.10	$(1.3 \pm 0.4) \times 10^{-3}$
$\Xi^0\bar{\Xi}^0 + \Xi^-\bar{\Xi}^+$	$\Lambda\bar{\Lambda}$	71 ± 12	0.05	$(3.2 \pm 0.8) \times 10^{-3}$
$\Xi^-\bar{\Xi}^+$	$\Xi^- + X$	51 ± 15	0.09	$(1.4 \pm 0.5) \times 10^{-3}$
$\Lambda\bar{\Sigma}^0 + \bar{\Lambda}\Sigma^0$	$\Lambda + X$	<20	0.33	$<1.5 \times 10^{-4}$

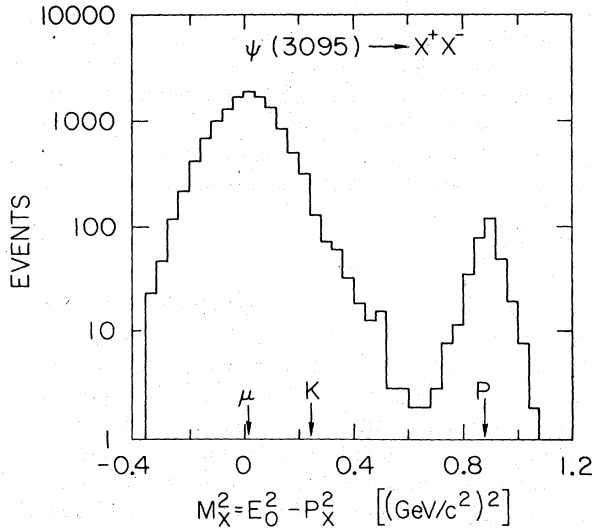


FIG. 4. Distribution of the invariant mass squared for two prong collinear, non- e^+e^- , tracks calculated from the energy of the incident beam and the measured momentum.

normalized to the same number of events. The two distributions agree well within the statistics. We have performed a fit to the proton angular distribution using a maximum likelihood technique and taking into account the geometrical efficiency of the apparatus. Using the fitting function $1 + \alpha \cos^2\theta$, we have obtained for α the value 1.45 ± 0.56 ,

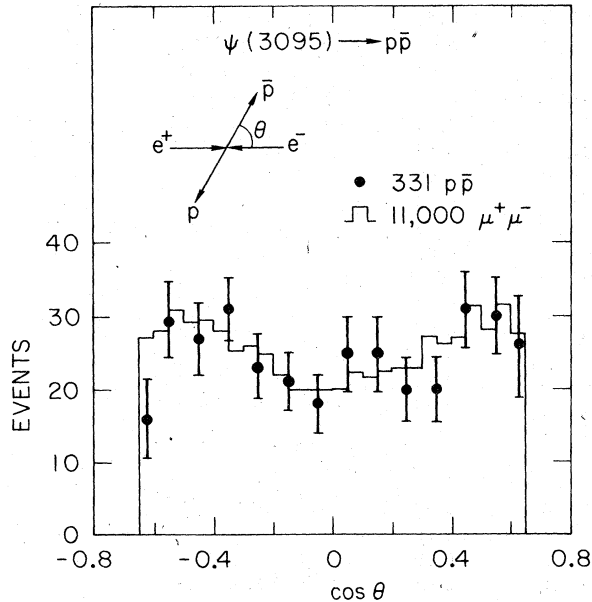


FIG. 5. Observed angular distribution of $p\bar{p}$ and $\mu^+\mu^-$ pairs with respect to the beam axis.

with a χ^2 of 0.48 per degree of freedom. As α can only vary in the range -1 to $+1$, we conclude from our measurement that α is close to $+1$. This means that the $p\bar{p}$ coupling is primarily of magnetic character, with at most a small electric contribution ("magnetic" and "electric" coupling in this case are the analog of G_M and G_E , respectively, for the virtual-photon- $p\bar{p}$ coupling).

B. $\psi \rightarrow p\bar{n}\pi^-$ and $\bar{p}n\pi^+$

To study this reaction we have selected two-prong events in which one track is compatible with being a proton; i.e., the TOF is that expected for a proton within 4 s.d. and the other track does not satisfy this criterion. The tracks are then assigned to be a proton and a pion, respectively, and the missing mass is calculated. Figure 6 shows the missing-mass distributions to the $p\pi^-$ and $\bar{p}\pi^+$, respectively. In both cases a clear peak is present at the neutron mass. These events come from the decay

$$\psi \rightarrow p\bar{n}\pi^- \quad (1)$$

and

$$\psi \rightarrow \bar{p}n\pi^+ \quad (2)$$

The number of events is 194 ± 17 for the $p\bar{n}\pi^-$ channel and 204 ± 18 for $\bar{p}n\pi^+$.

The efficiencies are respectively 0.22 and 0.25. (Events with a detected antiproton have higher triggering efficiency than corresponding events with detected protons.) The branching fractions are, respectively,

$$\frac{\Gamma(\psi \rightarrow p\bar{n}\pi^-)}{\Gamma(\psi \rightarrow \text{all})} = (2.16 \pm 0.29) \times 10^{-3},$$

$$\frac{\Gamma(\psi \rightarrow \bar{p}n\pi^+)}{\Gamma(\psi \rightarrow \text{all})} = (2.04 \pm 0.27) \times 10^{-3}.$$

We have investigated possible resonance formation in these $p\bar{n}\pi^-$ and $\bar{p}n\pi^+$ events. Figure 7 shows

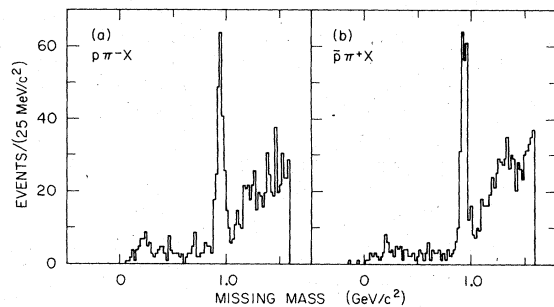


FIG. 6. Missing-mass spectrum in two-prong (a) $p\pi^-$ and (b) $\bar{p}\pi^+$ events.

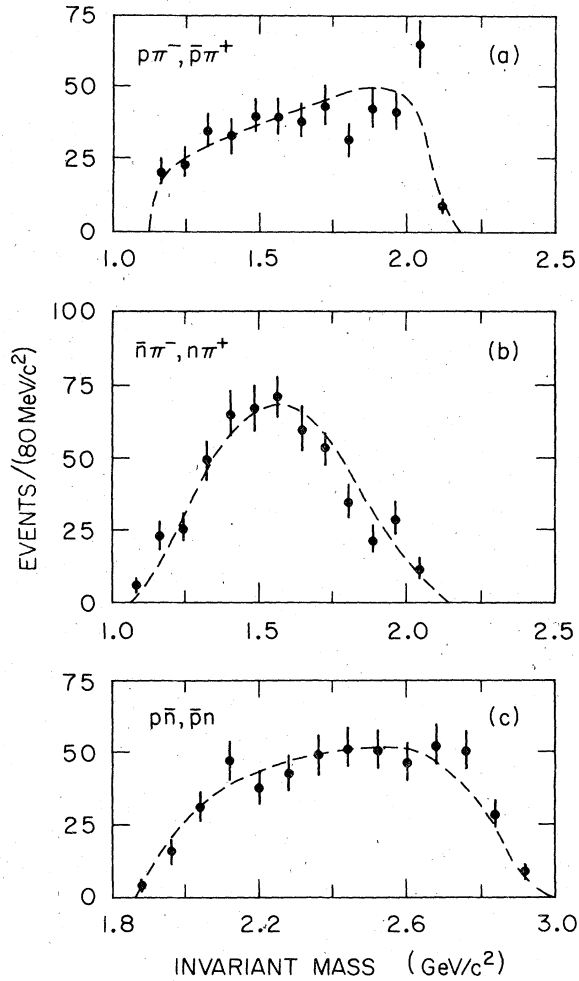


FIG. 7. Invariant-mass distributions for $p\bar{n}\pi^-$ and $\bar{p}n\pi^+$ events: (a) $p\pi^-$ and $\bar{p}\pi^+$ invariant mass, (b) $\bar{n}\pi^-$ and $n\pi^+$ invariant mass, and (c) $p\bar{n}$ and $\bar{p}n$ invariant mass. The difference in shape between parts (a) and (b) is due to differences in the acceptance.

the $N\bar{N}$ and $N\pi$ invariant mass distributions. The dotted lines are the Monte Carlo distribution obtained using the hypothesis of pure phase-space production. No clear structure is present in any of these distributions. In particular, there is no evidence for the isospin-violating decay $\psi \rightarrow \bar{\Delta}^0(1232)n$ at a level of about 5% of the $\psi \rightarrow \bar{p}n\pi^-$ rate.

C. $\psi \rightarrow p\bar{p}\pi^0, p\bar{p}\gamma$

To search for the decay into a $p\bar{p}$ pair plus a π^0 , we have selected two-prong noncollinear events in which both tracks are identified as protons by a 4-s.d. cut in the time of flight. If we assign the recoil mass to be that of a π^0 and then calculate the total invariant mass, we obtain the distribution

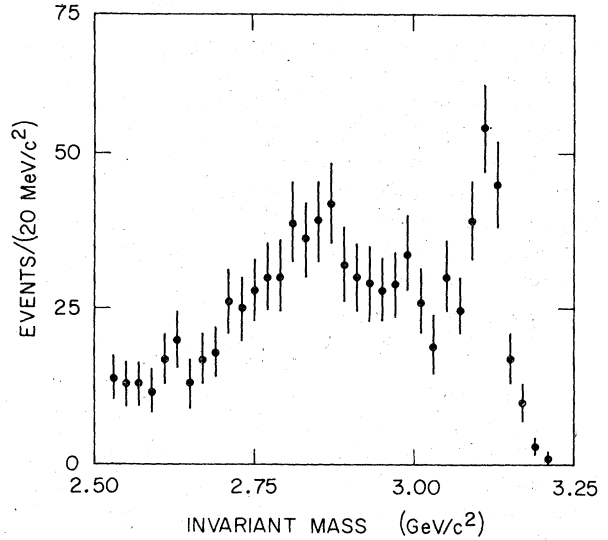


FIG. 8. Invariant-mass spectrum of $p\bar{p}\pi^0$ two-prong noncollinear events. Here the mass of the π^0 is assigned to the missing momentum.

shown in Fig. 8. The peak at the ψ mass corresponds to the decays

$$\psi \rightarrow p\bar{p}\pi^0 \quad (3)$$

and

$$\psi \rightarrow p\bar{p}\gamma. \quad (4)$$

Our missing-mass resolution is not sufficient by itself to allow the separation of the π^0 from the γ . The number of events in the peak is 109 ± 16 (smooth background subtracted). More information about these events can be obtained from the analysis of photons detected by the shower counters. Out of the 224 events in the peak region, 151 have a pulse in a shower counter which is approximately in the direction of the missing momentum. Three events have two shower-counter pulses which reconstruct the π^0 . Figure 9 shows the distribution of angle between the direction of the missing momentum and the photon (i.e., a pulse in the shower counter not associated with a track in the spark chambers) in the c.m. of the recoil system, which is assumed to be a pion. The latter distribution allows a discrimination between a missing γ or π^0 . In the case of a γ there should be a peak at zero degrees, while in the case of a π^0 there should be a flat distribution. The result of this analysis is that the angular distribution of photons is consistent with being due exclusively to process (3). The branching ratio calculated on the basis of 109 detected events is

$$\frac{\Gamma(\psi \rightarrow p\bar{p}\pi^0)}{\Gamma(\psi \rightarrow \text{all})} = (1.00 \pm 0.15) \times 10^{-3}.$$

From the measurement of reactions (1) and (2) we expect about 110 events from reaction (3) if the ψ has isospin 0.

To state an upper limit for reaction (4), we have fitted the angular distribution of Fig. 9(b) with a linear combination of the distributions expected from reactions (3) and (4). The result is that the upper limit for reaction (4), at 90% confidence level (C.L.), is 8 events. This corresponds to the following branching ratio upper limit:

$$\frac{\Gamma(\psi \rightarrow p\bar{p}\gamma)}{\Gamma(\psi \rightarrow \text{all})} < 1.1 \times 10^{-4} \text{ at } 90\% \text{ C.L.}$$

The $p\bar{p}$ invariant-mass distribution from all the events compatible with reaction (3) is shown in Fig. 10 and does not show any significant structure. From this distribution we can set an upper limit for the product: $B(\psi \rightarrow \gamma X(2830))B(X(2830) \rightarrow p\bar{p})$. In the region around 2.83 GeV there is no excess of events: If we make the unlikely assumption that all 8 events with invariant mass between 2.80 and 2.86 GeV/c are from the $X(2830)$ decay,¹⁰ then we derive the upper limit

$$B(\psi \rightarrow \gamma X(2830))B(X(2830) \rightarrow p\bar{p}) < 4 \times 10^{-5}.$$

In conclusion we have measured the branching ratios of decays (1), (2), and (3) and found that they are in very good agreement with the relative ratios predicted by the $I=0$ hypothesis: We also find that

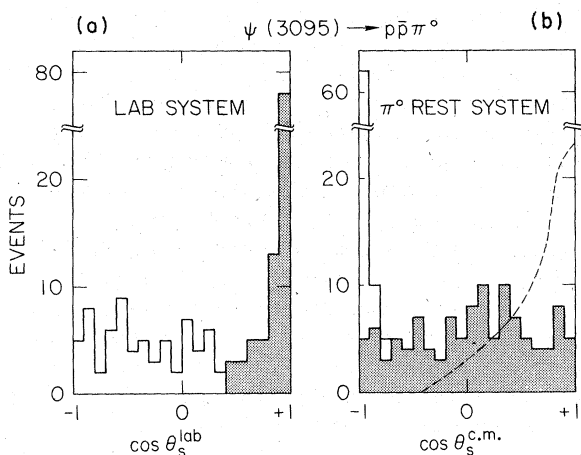


FIG. 9. Distribution of the angle between the direction of the missing momentum and the central direction of the shower for $p\bar{p}\pi^0$ or $p\bar{p}\gamma$ events (a) in the laboratory system and (b) in the c.m. of the π^0 . Note the break in the vertical scale. The shaded events are those with $\cos \theta$ in the laboratory system greater than 0.7. The unshaded events are consistent with being primarily background. The dashed line shows the predicted distribution if all of the shaded events were from the $p\bar{p}\gamma$ decay mode.

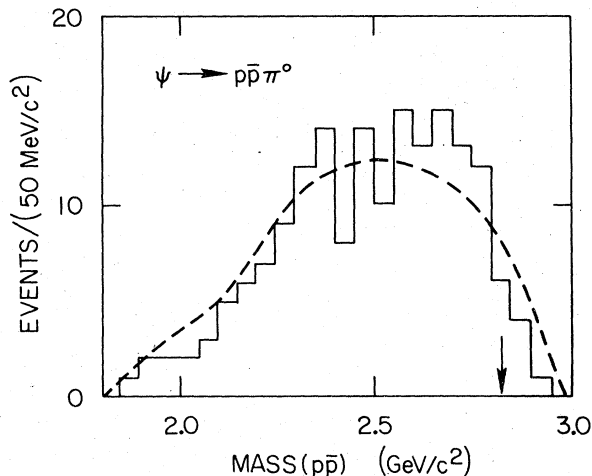


FIG. 10. Invariant-mass spectrum of the $p\bar{p}$ in $p\bar{p}\pi^0$ and $p\bar{p}\gamma$ events. The dashed line shows the phase-space distribution and the arrow indicates the mass of the $X(2830)$.

the final state $p\bar{p}\gamma$ has a branching ratio at least one order of magnitude lower than that for $p\bar{p}\pi^0$.

D. $\psi \rightarrow p\bar{p}\eta, p\bar{p}\omega, p\bar{p}\eta'$

The decay mode $\psi \rightarrow p\bar{p}\eta$ can be seen in our data as a peak centered at the η mass in the recoil mass distribution against a $p\bar{p}$ pair. This peak is more evident if only events with two detected prongs are considered, as in Fig. 11(a). This is a consequence of the fact that about 70% of the η decays involve all neutrals. The width of this peak is just what we expect from the resolution. The η peak in Fig. 11(a) contains 142 ± 19 events which translates into a branching ratio of $(2.3 \pm 0.34) \times 10^{-3}$, i.e., about the same magnitude as that for $\psi \rightarrow p\bar{p}$.

No significant peak, but only a small excess can be seen in Fig. 11(a) at the ω or η' mass. However, the efficiency is lower in this case by about a factor 5 because ω and η' decay preferably into charged particles, so that usually more charged tracks than the two protons are present in the detector. Figure 11(b) shows the recoil mass distribution against a $p\bar{p}$ pair when an additional pion is detected and more than one more pion is missing. (The recoil mass against the $p\bar{p}\pi$ system is required to be greater than 0.25 GeV to eliminate the process $\psi \rightarrow p\bar{p}\pi^+\pi^-$.) This distribution shows peaks at the η , ω , and η' mass; the number of events are 33 ± 10 , 42 ± 14 , and 19 ± 10 , respectively. Figure 11(c) shows the missing mass against the $p\bar{p}$ pair when two more pions are detected; the total momentum is required to be more than 0.1 GeV/c and events containing Λ candidates are rejected. This distribution is similar to the preceding one, with

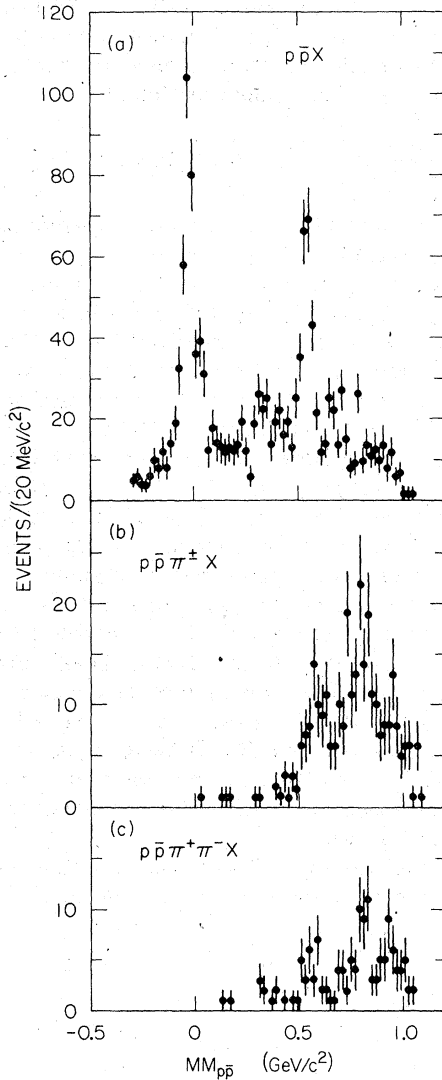


FIG. 11. Recoil-mass distribution against a $p\bar{p}$ pair in (a) two-prong $p\bar{p}$ events, (b) three-prong $p\bar{p}\pi^\pm$ events, and (c) Four-prong $p\bar{p}\pi^+\pi^-\pi^+\pi^-$ events.

the number of events being 22 ± 6 for $p\bar{p}\eta$, 35 ± 8 for $p\bar{p}\omega$, and 21 ± 8 for $p\bar{p}\eta'$. The measurements in the three and four detected prong topologies are consistent with the respective efficiencies for all three processes. Therefore in order to obtain the branching ratios we combine both topologies. The results are

$$\frac{\Gamma(\psi \rightarrow p\bar{p}\omega)}{\Gamma(\psi \rightarrow \text{all})} = (1.6 \pm 0.3) \times 10^{-3}$$

and

$$\frac{\Gamma(\psi \rightarrow p\bar{p}\eta')}{\Gamma(\psi \rightarrow \text{all})} = (1.8 \pm 0.6) \times 10^{-3}.$$

In the case of the $p\bar{p}\eta'$ decay the quoted error re-

flects the sizable uncertainty in the background subtraction due to the location of the peak just at the edge of the phase-space distribution.

E. $\psi \rightarrow p\bar{p}\pi^+\pi^-$

The decay $\psi \rightarrow p\bar{p}\pi^+\pi^-$ is clearly seen in four-prong events with a $p\bar{p}$ pair identified by TOF, and kinematically fully reconstructed. Figure 12(a) shows the invariant mass of the four-prong events, with one $p\bar{p}$ pair identified by TOF, once all the events containing Λ candidates have been removed. The presence of the peak at the ψ mass, with width compatible with the resolution, establishes the existence of the decay $p\bar{p}\pi^+\pi^-$. The number of the events can be extracted more readily from Fig. 13, where the correlation between invariant mass and total momentum is plotted for

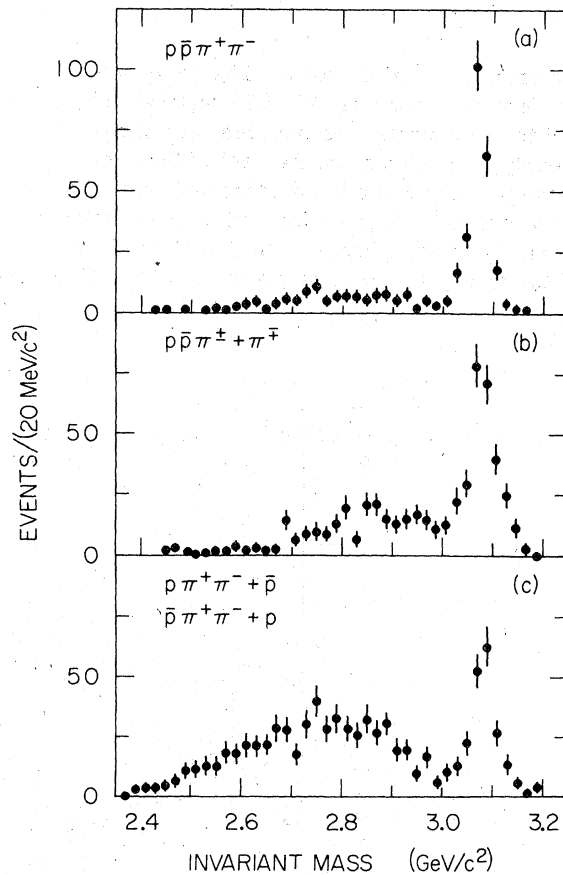


FIG. 12. Invariant-mass spectrum of $p\bar{p}\pi^+\pi^-$ combinations in (a) events in which all four prongs are observed, (b) events in which a p , \bar{p} , and π^\pm are observed and the π mass is assigned to the missing momentum, and (c) events in which a π^+ , π^- , and either a p or \bar{p} are seen and the p mass is assigned to the missing momentum.

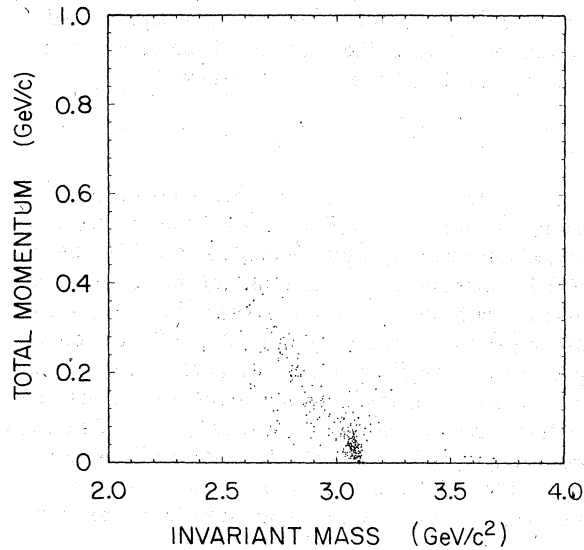


FIG. 13. Correlation between total invariant mass and total momentum for four-prong $p\bar{p}\pi^+\pi^-$ events.

the same sample of events. The decay into $p\bar{p}\pi^+\pi^-$ produces a cluster of 220 ± 16 events at the ψ mass and total momentum compatible with zero which is clearly separated from the rest of the events. The same process can also be identified from the category of three-prong events with a one constraint fit on the missing mass: We find 135 ± 24 events of the type $p\pi\pi +$ missing proton and 178 ± 25 events

of the type $p\bar{p}\pi^+ +$ missing pion [Figs. 12(b) and 12(c); in both cases all events containing a Λ^0 candidate were excluded]. These measurements translate into a branching fraction of

$$\frac{\Gamma(\psi \rightarrow p\bar{p}\pi^+\pi^-)}{\Gamma(\psi \rightarrow \text{all})} = (5.5 \pm 0.6) \times 10^{-3}.$$

We have investigated the possible presence of resonant structure between the four particles of this process. Figure 14 shows the invariant mass for the $(p\pi)^0$, $(p\pi)^{\pm\pm}$, $p\bar{p}$, $\pi^+\pi^-$ pairs in the events corresponding to a $p\bar{p}\pi^+\pi^-$ decay of the ψ . The dotted curves represent the distributions expected from phase space. The $(p\pi)^{\pm\pm}$ distribution shows a clear Δ^{++} or $\bar{\Delta}^{--}$ signal of 263 ± 22 events above the phase-space distribution. Thus about 25% of the protons (or antiprotons) in the $p\bar{p}\pi^+\pi^-$ final state come from the decay of a Δ^{++} or $\bar{\Delta}^{--}$. A study of the correlation of the momentum and the invariant mass of the $p\pi^+$ ($\bar{p}\pi^-$) pairs shows an excess of events in the region corresponding to $\Delta^+\bar{\Delta}^-$ pair production when compared with uncorrelated production simulated by Monte Carlo. Qualitatively the process $\psi \rightarrow \Delta^+\bar{\Delta}^-$ could account for as much as 15% of the $p\bar{p}\pi^+\pi^-$ mode. A more precise evaluation of this effect is difficult because the Δ is too wide and the Δ mass is close to the maximum of the phase-space distribution for uncorrelated $p\bar{p}\pi^+\pi^-$ production.

Comparison of the $p\pi^-$ ($\bar{p}\pi^+$) mass distribution with the Monte Carlo for uncorrelated $p\bar{p}\pi^+\pi^-$ decay

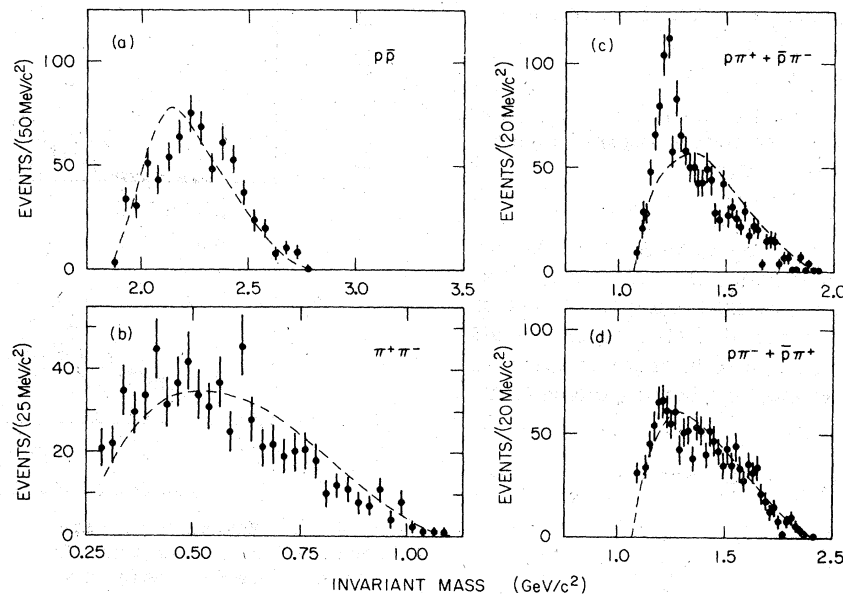


FIG. 14. Invariant-mass spectra of different particle combinations for $p\bar{p}\pi^+\pi^-$ events with total momentum less than $100 \text{ MeV}/c^2$.

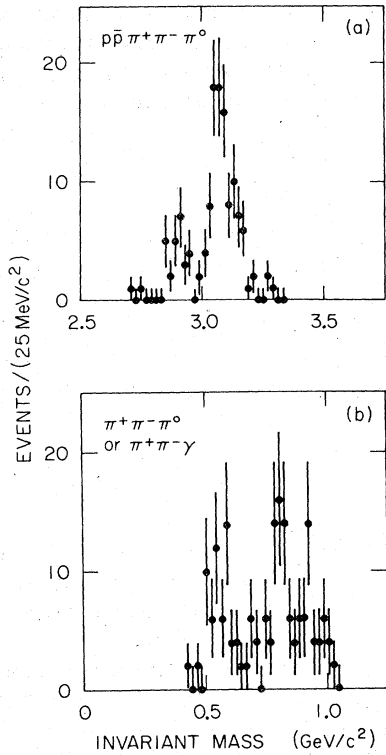


FIG. 15. (a) Invariant-mass distribution of $p\bar{p}\pi^+\pi^-\pi^0$ combinations observed using $p\bar{p}\pi^+\pi^-\pi^0$ events with missing momentum, (b) missing-mass distribution against the $p\bar{p}$ pair in the events in the peak at the ψ mass in (a).

also shows an excess of events in the mass region of the Δ^0 ($\bar{\Delta}^0$). This signal appears smaller because the Δ^0 decays to $p\pi^-$ only one-third of the time.

F. $\psi \rightarrow \Lambda\bar{\Lambda}$

Most of the events with a p , \bar{p} , π^+ , and π^- detected which are not due to $\psi \rightarrow p\bar{p}\pi^+\pi^-$ satisfy the hypothesis of having a π^0 missing. Figure 15 shows the total invariant-mass distribution when the π^0 mass is assigned to the recoil momentum. Analysis of the $\pi^+\pi^-\pi^0$ mass distribution for events in the peak at the ψ mass shows that 22 ± 5 are from the decay $p\bar{p}\eta$, 25 ± 5 from $p\bar{p}\omega$, 6 ± 2 from $p\bar{p}\eta'$, and the remaining 39 ± 14 attributed to other decays of the form

$$\psi \rightarrow p\bar{p}\pi^+\pi^-\pi^0$$

and

$$\psi \rightarrow p\bar{p}\pi^+\pi^-\gamma.$$

The branching ratio corresponding to these 39 events is $(1.6 \pm 0.6) \times 10^{-3}$.

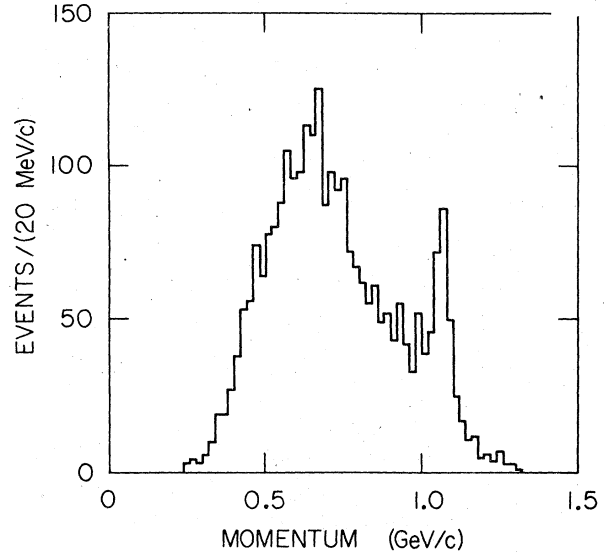


FIG. 16. Momentum distribution for all Λ or $\bar{\Lambda}$ candidates.

VI. DECAYS INVOLVING STRANGE BARYONS

A. $\psi \rightarrow \Lambda\bar{\Lambda}$

We have described in Sec. III the technique we use to identify a Λ (or $\bar{\Lambda}$) in our data. We will describe in this section the results obtained in the analysis of the events containing at least one measured Λ or $\bar{\Lambda}$.

The momentum distribution of the $\Lambda + \bar{\Lambda}$ sample is shown in Fig. 16. The peak centered at 1.07 GeV/c corresponds to the decay $\psi \rightarrow \Lambda\bar{\Lambda}$. This same

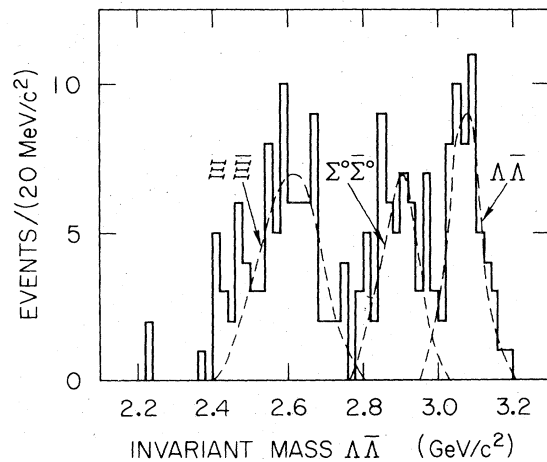


FIG. 17. Invariant-mass spectrum of the $\Lambda\bar{\Lambda}$ in all events containing a $\Lambda\bar{\Lambda}$ pair. The dashed lines show the expected distributions from $\Lambda\bar{\Lambda}$, $\Sigma^0\bar{\Sigma}^0$, and $\Xi\bar{\Xi}$ decay modes.

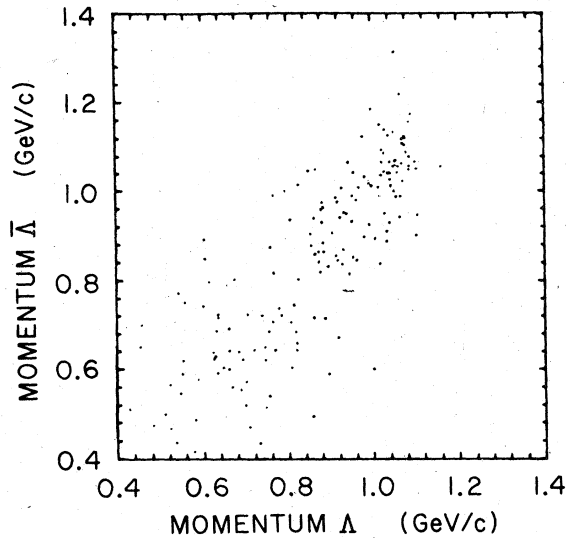


FIG. 18. Λ momentum versus $\bar{\Lambda}$ momentum for all events containing a $\Lambda\bar{\Lambda}$ pair.

process can be measured using the sample of events with both a Λ and $\bar{\Lambda}$ reconstructed. In fact, the invariant-mass distribution of the $\Lambda\bar{\Lambda}$ pair has a peak centered at the ψ mass (Fig. 17), and the correlation between the momentum of the Λ versus the momentum of the $\bar{\Lambda}$ cluster around 1.07 GeV/c (Fig. 18). The peak in the inclusive Λ momentum distribution has 153 ± 24 events after a smooth background subtraction. In the sample of events containing both a detected Λ and $\bar{\Lambda}$ there are 43 ± 8

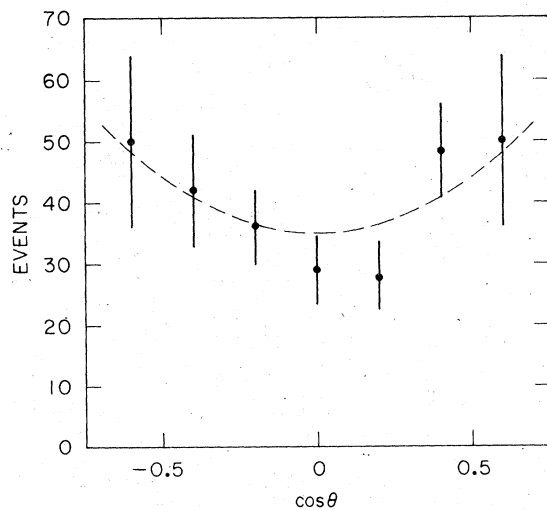


FIG. 19. Angular distribution of the $\Lambda\bar{\Lambda}$ collinear pair with respect to beam axis, corrected for the detector acceptance. The dashed curve shows a $1 + \cos^2\theta$ distribution.

events kinematically compatible with pair production. Taking into account the efficiencies, these two measurements are in very good agreement and give the following branching ratio:

$$\frac{\Gamma(\psi \rightarrow \Lambda\bar{\Lambda})}{\Gamma(\psi \rightarrow \text{all})} = (1.1 \pm 0.2) \times 10^{-3}.$$

Figure 19 shows the angular distribution of the Λ 's with momentum between 1.04 and 1.10 GeV/c, corrected for the angular acceptance of the detector. The agreement with the hypothesis $1 + \cos^2\theta$ is good (the χ^2 is 8 for 14 DOF). We note that if the ψ has the properties of an SU(3) singlet we expect the same behavior for the $p\bar{p}$ and $\Lambda\bar{\Lambda}$ angular distribution.

$$B. \psi \rightarrow \Lambda\bar{\Sigma}, \Sigma\bar{\Sigma}, \Xi\bar{\Xi}, \text{etc.}$$

Λ 's from the decay $\psi \rightarrow \Lambda\bar{\Lambda}$ account for only a fraction of the detected Λ 's; from the kinematic properties of the Λ 's we can get information about more complicated reactions producing Λ 's in the final state.

From the analysis of the Λ momentum spectrum we can conclude that there is no clear evidence for other two-body decays of the kind $\psi \rightarrow \Lambda X$. In particular, we note that there is no evidence for the $I = 1 \Lambda\bar{\Sigma}^0$ or $\bar{\Lambda}\Sigma^0$ final states which would produce a peak at $P_\Lambda = 1.03$ GeV/c. There is a slight excess in the region $p_\Lambda \approx 0.6$ GeV/c which corresponds to $M(X) = 1.670$ GeV. Although a Λ^* exists at about this mass, this process cannot be clearly

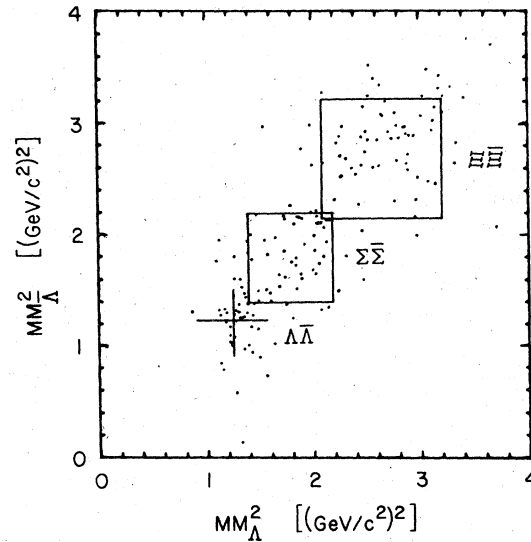


FIG. 20. Missing mass squared against the Λ versus missing mass squared against the $\bar{\Lambda}$ for all events containing a $\Lambda\bar{\Lambda}$ pair. The boxes show the kinematic limits for $\Sigma^0\bar{\Sigma}^0$ and $\Xi\bar{\Xi}$ decay modes.

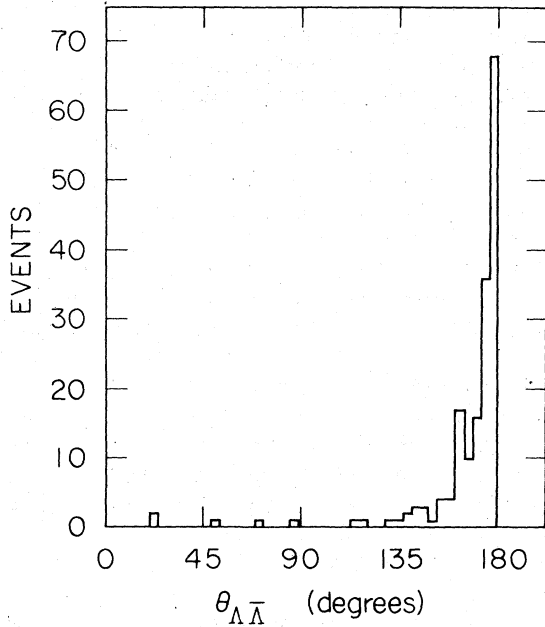


FIG. 21. Opening-angle distribution between the Λ and the $\bar{\Lambda}$ for all events containing a $\Lambda\bar{\Lambda}$ pair.

separated with the statistics available for this analysis.

More information can be obtained by studying the sample of events in which both the Λ and $\bar{\Lambda}$ are detected. Figure 20 shows the correlation between the missing mass squared against the Λ and the $\bar{\Lambda}$, respectively. The events group in three categories, one of which corresponds to $\Lambda\bar{\Lambda}$ pair production. The rest of the events are mainly in the regions kinematically compatible with $\Sigma^0\bar{\Sigma}^0$, $\Xi^-\bar{\Xi}^+$, and $\Xi^0\bar{\Xi}^0$ production. Inelastic processes such as $\Lambda\bar{\Lambda}\pi^0$, $\Lambda\bar{\Lambda}\pi^+\pi^-$, $\Lambda\bar{\Lambda}\pi^0\pi^0$, and $\Lambda\bar{\Sigma}\pi^0$ have large regions of overlap with the previous reactions; however, the observed events populate only the regions which correspond to Σ and Ξ pair production. Another indication that these pair-production processes are favored comes from the study of the angle between the Λ and $\bar{\Lambda}$ directions. This distribution, shown in Fig. 21, is strongly peaked at 180° ; out of 198 events, 196 have $\cos\theta < -0.8$ while inelastic states with additional π 's or γ 's should have a much broader distribution. Assuming that the $\Lambda\bar{\Lambda}$ inelastic pairs which we observe in the kinematical regions compatible with Σ and Ξ pair production come from these processes, we have the following branching fractions:

$$\frac{\Gamma(\psi \rightarrow \Sigma^0\bar{\Sigma}^0)}{\Gamma(\psi \rightarrow \text{all})} = (1.3 \pm 0.4) \times 10^{-3}$$

and

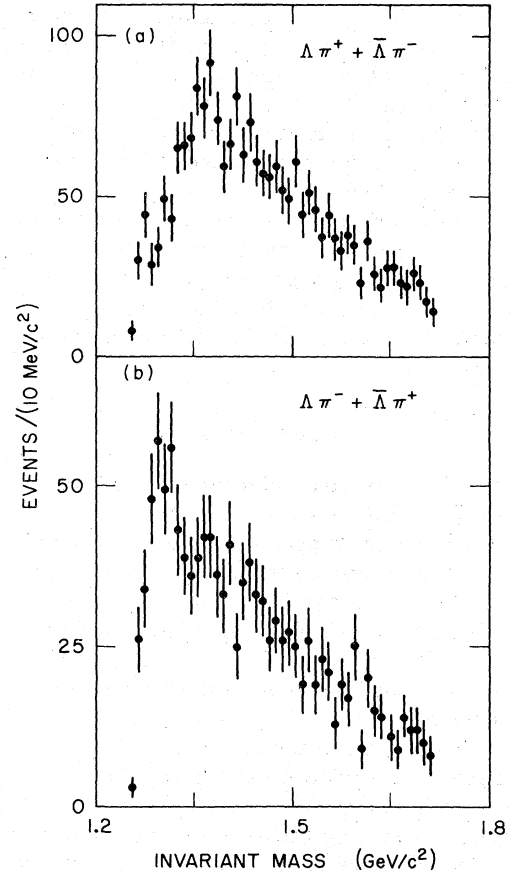


FIG. 22. Invariant-mass spectra of (a) $\Lambda\pi^+$ and $\bar{\Lambda}\pi^-$, and (b) $\Lambda\pi^-$ and $\bar{\Lambda}\pi^+$ combinations.

$$\frac{\Gamma(\psi \rightarrow \Xi^-\bar{\Xi}^+)}{\Gamma(\psi \rightarrow \text{all})} = (3.2 \pm 0.8) \times 10^{-3}.$$

We have also direct evidence of Ξ^- ($\bar{\Xi}^+$) production from the ψ from the study of the invariant mass of $\Lambda\pi^-$ ($\bar{\Lambda}\pi^+$). Figure 22 shows the $\Lambda\pi^-$ ($\bar{\Lambda}\pi^+$) invariant-mass distributions. A signal is clearly visible in the former with 153 ± 22 events in the peak. Studying the correlation between $\Lambda\pi^-$ ($\bar{\Lambda}\pi^+$) invariant mass and missing mass, we find in fact an excess of events in the region corresponding to $\Xi^-\bar{\Xi}^+$ production. This measurement, taking into account the efficiency to detect a single Ξ from this reaction, translates into a branching fraction of

$$\frac{\Gamma(\psi \rightarrow \Xi^-\bar{\Xi}^+)}{\Gamma(\psi \rightarrow \text{all})} = (1.4 \pm 0.5) \times 10^{-3}.$$

This is consistent with being one-half of the previous measurement of the sum of $\Xi^0\bar{\Xi}^0$ and $\Xi^-\bar{\Xi}^+$ production.

Finally we note that the sum of the exclusive pro-

cesses for which we have measured the branching fraction accounts for only about 50% of all the detected Λ 's. The remaining Λ 's could come from modes such as $\Lambda\Sigma\pi$, $\Sigma^0\bar{\Sigma}\pi$, $\Lambda\bar{N}K$, etc. We do not quote an inclusive fraction for decays containing a Λ because the efficiency depends strongly on the nature of the final state.

The results we have described in this section are summarized in Table I. The branching fraction for Σ and Ξ pair production may be overestimated, as we have attributed all the events kinematically compatible with these processes as due to them.

VII. SUMMARY

We have measured a number of branching ratios for the decay of the ψ into baryonic modes. The number of detected protons per event is much higher at the ψ energy than in e^+e^- production off resonance, and these final states therefore cannot be attributed to second-order electromagnetic processes.

We have added more evidence for the $I=0$ assignment for the ψ :

(a) There is a substantial $\Lambda\bar{\Lambda}$ decay mode, whereas there is no evidence for ψ decays to $I=1$ final states such as $N\bar{\Delta}$, $\bar{\Lambda}\bar{\Sigma}^0$, or $\Lambda\bar{\Lambda}\pi^0$.

(b) The branching ratios to the final states $p\bar{n}\pi^-$, $\bar{p}n\pi^+$, and $p\bar{p}\pi^0$ are in the ratio 2:2:1, as expected

for the $I=0$ assignment.

The $p\bar{p}$ and the $\Lambda\bar{\Lambda}$ pair from $\psi \rightarrow p\bar{p}$ and $\psi \rightarrow \Lambda\bar{\Lambda}$, respectively, have within statistics the same angular distribution. The fact that this distribution is of the type $1 + \cos^2\theta$ demonstrates that the coupling of the ψ to baryon-antibaryon pairs is of magnetic rather than electric character.

If the ψ is an SU(3) singlet decaying via an SU(3)-symmetric interaction, the ratio $r = \Gamma(\psi \rightarrow \Lambda\bar{\Lambda}) / \Gamma(\psi \rightarrow p\bar{p})$ should be ~ 0.9 for an S wave and ~ 0.5 for a D wave. From the angular distribution measurement, we know that it is a coherent mixture of the two which should give $r \sim 0.74$. Our result $r = 0.5 \pm 0.1$ is slightly lower than the SU(3) prediction.

We have shown evidence that the final states $p\bar{p}$, $p\bar{p}\eta$, $p\bar{p}\omega$, $p\bar{p}\pi^0$, $p\bar{p}\eta'$ are produced with comparable branching ratios. We do not have evidence that the η and the η' mesons are preferred with respect to the π^0 or the ω , although the phase space for the decay $\psi \rightarrow p\bar{p}\eta'$ is considerably smaller than for the others.

We have also shown that the $p\bar{p}\pi^+\pi^-$ state has the highest branching ratio of all the states containing baryons, and a non-negligible fraction has a p and π resonant as a Δ .

It is of some interest to examine what can be inferred from the specific observed states about the population of states with the same particle multiplicities but different (and unobservable in our apparatus) charge combinations. For this purpose

TABLE II. Branching ratios B into general modes computed from the observation of one particular charge state of that mode.

Observed	General Mode	Statistical model			
		$\frac{B(\text{observed})}{B(\text{general})}$	$B(\text{general})$ (%)	$\frac{B(\text{observed})}{B(\text{general})}$	$B(\text{general})$ (%)
$p\bar{p}$	$N\bar{N}$	$\frac{1}{2}$	0.44 ± 0.04	$\frac{1}{2}$	0.44 ± 0.03
$p\bar{n}\pi^-$	$N\bar{N}\pi$	$\frac{5}{6}$	0.62 ± 0.05	$\frac{5}{6}$	0.62 ± 0.05
$\bar{p}n\pi^+$					
$p\bar{p}\pi^0$					
$p\bar{p}\eta$	$N\bar{N}\eta$	$\frac{1}{2}$	0.46 ± 0.08	$\frac{1}{2}$	0.46 ± 0.07
$p\bar{p}\omega$	$N\bar{N}\omega$	$\frac{1}{2}$	0.32 ± 0.06	$\frac{1}{2}$	0.32 ± 0.12
$p\bar{p}\eta'$	$N\bar{N}\eta'$	$\frac{1}{2}$	0.36 ± 0.12	$\frac{1}{2}$	0.36 ± 0.12
$p\bar{p}\pi^+\pi^-$	$N\bar{N}\pi\pi$	$\frac{1}{6} - \frac{1}{3}$	1.65 ± 0.18 to 3.30 ± 0.36	$\frac{1}{4}$	2.20 ± 0.24
$p\bar{p}\pi^+\pi^-\pi^0$	$N\bar{N}\pi\pi\pi$	$\frac{1}{15} - \frac{1}{2}$	0.32 ± 0.12 to 2.40 ± 0.90	$\frac{9}{40}$	0.72 ± 0.27
$\Lambda\bar{\Lambda}$	$\Lambda\bar{\Lambda}$	1	0.11 ± 0.02	1	0.11 ± 0.02
$\Sigma^0\bar{\Sigma}^0$	$\Sigma\bar{\Sigma}$	$\frac{1}{3}$	0.39 ± 0.12	$\frac{1}{3}$	0.39 ± 0.12
$\Xi^0\bar{\Xi}^0$	$\Xi\bar{\Xi}$	1	0.32 ± 0.08	1	0.32 ± 0.08
$\Xi^-\bar{\Xi}^+$					
Total			5.0 ± 0.3 to 8.7 ± 1.0		5.9 ± 0.4

we use the known zero isospin of the ψ and isospin conservation in the decay process to calculate the ratio between the observed state and the sum of all states with the same multiplicity and particles in all charge combinations.^{11,12} In some cases only limits can be obtained, and the range of the allowed values is rather broad. Using the statistical model¹³ in which all available isospin states are populated in proportion to their statistical weights, we can obtain a unique prediction. Table II contains the results of this analysis.

The sum of branching-ratio lower limits for ψ decays into states containing a baryon pair discussed in this paper is $(5.0 \pm 0.3)\%$; if the statistical model is assumed, the total branching ratio is $(5.9 \pm 0.4)\%$.

This latter number can be added to the (30.2

$\pm 3.3\%$) of ψ decays which were accounted for by the statistical model on the basis of measurement of mesonic decay modes.⁴ This total of $(36.1 \pm 3.3)\%$ of ψ decays should be compared to the 69% of ψ decays which do not arise from second-order electromagnetic processes.¹⁴ The 33% of ψ decays which are currently unaccounted for are presumably decays with higher multiplicities and decays involving photons and/or η 's.

ACKNOWLEDGMENTS

We wish to thank F. J. Gilman for informative discussions and useful suggestions. This work was supported by the U. S. Department of Energy. One of us (D. Lücke) would like to thank Deutsche Forschungsgemeinschaft for financial support.

*Present address: Laboratori Nazionali di Frascati dell'INFN, Rome, Italy.

†Present address: DESY, Hamburg, Germany.

‡Present address: Harvard University, Cambridge, Mass.

§Present address: CERN, Geneva, Switzerland.

¶Permanent address: LPNHE, Université Paris VI, Paris, France.

||Present address: University of Illinois, Urbana, Illinois.

¹G. Goldhaber *et al.*, Phys. Rev. Lett. 37, 255 (1976);

I. Peruzzi *et al.*, *ibid.* 37, 569 (1976).

²G. J. Feldman *et al.*, Phys. Rev. Lett. 38, 1313 (1977);

G. Goldhaber *et al.*, Phys. Lett. 69B, 503 (1977).

³B. Jean-Marie *et al.*, Phys. Rev. Lett. 36, 291 (1976).

⁴F. Vannucci *et al.*, Phys. Rev. D 15, 1814 (1977).

⁵H. Harari, Phys. Rev. Lett. 60B, 172 (1976).

⁶J.-E. Augustin *et al.*, Phys. Rev. Lett. 34, 233 (1975).

⁷G. Goldhaber *et al.*, in *Proceedings of the Fourth International Symposium on NN Interactions, Syracuse, New York, 1975*, edited by T. E. Kalogeropoulos and K. C. Wali (Syracuse Univ., Syracuse, 1975).

⁸W. Braunschweig *et al.*, Phys. Lett. 63B, 487 (1976).

⁹L. Criegee *et al.*, DESY Report No. 75/32, 1975 (unpublished).

¹⁰W. Braunschweig *et al.*, Phys. Lett. 67B, 243 (1977).

¹¹I. M. Shmushkevich, Dokl. Akad. Nauk SSSR 103, 235 (1955).

¹²A. Pais, Phys. Rev. Lett. 32, 1081 (1974). Also see M. Peshkin and J. Rosner, Nucl. Phys. B122, 144 (1977).

¹³A. Pais, Ann. Phys. (N.Y.) 9, 548 (1960).

¹⁴A. M. Boyarski *et al.*, Phys. Rev. Lett. 34, 1357 (1975).